Underwater hyperspectral imagery for Posidonia oceanica mapping: challenges and preliminary results from the POSEIDON Project

Valeria Longhi [1], Nives Grasso[2], Paolo Felice Maschio[2], Fabio Menna[3], Arianna Pansini[3], Andrea Maria Lingua[2], Filiberto Chiabrando[4], Erica Nocerino[5], Giulia Ceccherelli[3], Sabrina Rossi[6]

[1] Interuniversity Department of Regional and Urban Studies and Planning (DIST), Politecnico di Torino, Italy – valeria.longhi@polito.it
[2] Department of Environment, Land and Infrastructure Engineering (DIATI), Politecnico di Torino, Italy – (nives.grasso, andrea.lingua, paolo.maschio)@polito.it
[3] Department of Chemical, Physical, Mathematical and Natural Sciences, University of Sassari, Italy – (fmenna, apansini, cecche@uniss.it)
[4] Department of Architecture and Design (DAD) Politecnico di Torino, Italy – filiberto.chiabrando@polito.it
[5] Department of Humanities and Social Sciences, University of Sassari, Italy - enocerino@uniss.it
[6] Biru srl, Italy - rossi@culuccia.org

Keywords: Hyperspectral imagery, Posidonia oceanica, Underwater surveying, Seagrass mapping, Spectral signature analysis.

Abstract

Posidonia oceanica (PO) meadows are important ecosystems in the Mediterranean, supporting biodiversity and ecosystem services, yet they face increasing threats due to anthropogenic pressures and climate change. To address these challenges, the POSEIDON project aims to develop ultra-high-resolution (UHR) and beyond ultra-high-resolution (BUHR) mapping methods for PO monitoring. This study focuses on underwater hyperspectral imagery (UHI) as a tool to complement and support the standard monitoring protocols established by ISPRA. Data were collected along the northern coast of Sardinia, with hyperspectral acquisitions performed both underwater, at depths of 5–15 meters, and out of the water, over collected samples, using a Senop Rikola hyperspectral camera. The study faced several challenges, including image blurring due to the movement of seagrass and light absorption by water, which limits the effectiveness of infrared bands. Despite these difficulties, the preliminary tests provided valuable insights into the system's limitations and suggested improvements for future data acquisition. This paper outlines the methodology, presents initial results, and discusses strategies to enhance underwater hyperspectral data quality for future monitoring efforts.

1. Introduction

Posidonia oceanica (PO) meadows are among the most valuable coastal ecosystems in the Mediterranean Sea, playing a crucial role in ecosystem services and functioning (Vassallo et al., 2013). Recognised as a biological indicator under the EU Water Framework Directive, PO meadows serve as nursery and forage areas for numerous species, including commercially significant fish and crustaceans (Mazzuca et al., 2009). However, in recent decades, PO has faced increasing threats, with widespread die-offs attributed to anthropogenic pressures and climate change. These concerns have driven the demand for high-resolution mapping and innovative methodologies to complement traditional monitoring techniques.

The POSEIDON project, funded by the National Recovery and Resilience Plan (PNRR), addresses these challenges by developing and testing ultra-high-resolution (UHR) and beyond ultra-high-resolution (BUHR) mapping methods. The project aligns with international conservation efforts through the Save the Wave initiative, including European Environmental Directives, the Mediterranean PO Network, the International Partnership for Blue Carbon, and UNESCO's Intergovernmental Oceanographic Commission.

As part of POSEIDON, different research groups are exploring diverse technologies for PO mapping. This contribution focuses on the application of underwater hyperspectral imagery (UHI) for PO monitoring. The study employs the Senop Rikola hyperspectral camera, a snapshot imaging system based on a Fabry–Pérot interferometer, covering the 500–900 nm spectral range with 1 nm resolution. The objective is to provide complementary tools to support the standard Italian monitoring protocol established by ISPRA (Istituto Superiore per la Protezione e la Ricerca Ambientale).

1.1 Related works

Few studies have examined hyperspectral data's application in understanding marine plant species, emphasizing its potential for non-invasive, high-resolution monitoring. Some research has utilized point-based reflectance measurements from spectrometers, mainly focusing on seagrass and macroalgae. For example, researchers have used hyperspectral signatures of Zostera noltei to estimate aboveground biomass through both field and laboratory methods, identifying vegetation indices like NDVI-705 as effective non-destructive measures for monitoring biomass across seasons (Costa et al., 2021). Likewise, hyperspectral reflectance profiles have been utilized to differentiate invasive Caulerpa species from native algae, indicating potential for species-level classification in management settings (Kišević et al., 2011). However, these studies focus on point-based data acquisition instead of using full hyperspectral imagery. A different line of research has emerged, using underwater hyperspectral imagers (UHI) mounted on remotely operated vehicles (ROVs) or operated by divers. These systems enable the acquisition of spatially continuous hyperspectral images, facilitating the precise mapping and categorization of seafloor habitats and benthic organisms according to their optical characteristics. Illustrative applications include the mapping of coral reefs, kelp forests, cold-water coral habitats, and manganese nodules, as well as experimental setups for classifying seabeds and monitoring benthic communities using machine-learning processes (Dumke

et al., 2018; Foglini et al., 2019; Johnsen et al., 2016; Mills et al., 2023). These contributions collectively indicate that hyperspectral imaging is a valuable tool for mapping seagrass and macroalgae, with increasing importance for conservation and policy frameworks.

1.2 Challenges and Research Questions

The study raises key questions regarding the feasibility of hyperspectral imaging for assessing vegetation health underwater. While this technology is well established for terrestrial vegetation, its adaptation to the underwater environment presents significant challenges, including:

- The strong absorption of light in water, which limits the effectiveness of infrared bands.
- The constant motion of seagrass due to water dynamics, complicating image acquisition.
- The need for improved acquisition protocols to mitigate image blurring and enhance spectral data reliability.

2. Materials and methods

2.1 The underwater hyperspectral imaging(UHI) system

The methodology proposed for seagrass analysis is carried out using a hyperspectral camera, the Senop Rikola (Figure 1). Through this tool, the goal is to support and complement ISPRA's monitoring steps, trying to assess the health status of the PO, and its stress level.

Rikola is a snapshot camera based on a Fabry–Pérot interferometer (FPI) and on a dual sensor configuration. The two orthogonally placed complementary metal-oxide-semiconductor (CMOS) sensors are responsible for acquiring different spectral ranges: Sensor 1, captures the spectral range of 500–630 nm (VIS) and Sensor 2 captures the range of 650–900 nm (NIR). A beam-splitting prism splits the light ray for the two sensors. These internal components of the camera are depicted in a diagram in Figure 1.

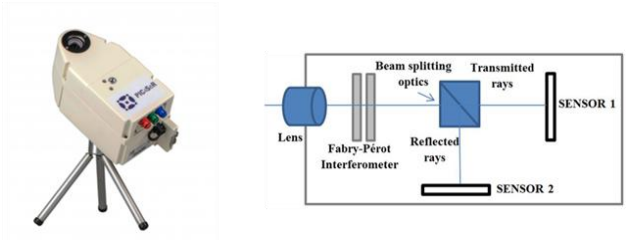

Figure 1. Rikola hyperspectral camera and a diagram of its internal geometry (Tommaselli et al., 2016).

The camera has a field of view (FOV) of about 35◦, producing images with 1010 x 1010 pixels, with a pixel size of 5.5 µm and a focal length of 8.7 mm. The Rikola can be used building a sequence of wavelengths to be recorded by the camera. The camera can take pictures in different wavelength bands, ranging from 500 to 900 nm, with a spectral resolution of 1 nm. Usually, hyperspectral study of vegetation relies on wavelengths ranging from 700 nm to 800 nm, in the near infrared band, where plants exhibit their reflectance peak. The raw data are stored on a Compact Flash card in autonomous mode, which will be converted to radiance using the Rikola Hyperspectral Imager software. In order to do that in the processing phase, calibration targets with known reflectance in the whole spectrum are used during the acquisition.

To allow underwater acquisition, a waterproof housing has been designed and built ad hoc by the Geomatic Laboratories of DIATI[1] and DAD[2] departments of Politecnico di Torino. In addition, two halogen lamps illuminate the full spectrum of the hyperspectral camera (Figure 2). The initial version of the acquisition setup is finalised by placing this system, which includes the camera, housing, and lights, on a tripod to achieve a more stable acquisition underwater.

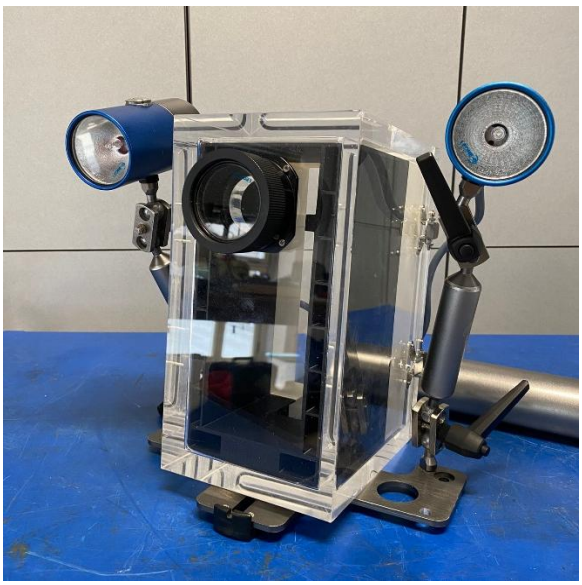

Figure 2. Rikola's waterproof case and the initial version of the artificial lighting system, currently under improvements.

2.2 Preliminary laboratory tests

A series of laboratory tests were conducted to determine the optimal camera-object distance for acquiring well-focused underwater images using the UHI system. These tests aimed to evaluate the performance of the Rikola camera within its waterproof flat-port housing and to assess the resulting spatial resolution at different working distances. Laboratory results indicated that the shortest camera-to-object distance for obtaining in-focus pictures in underwater conditions is approximately 50 cm. Considering the acquisition takes place on the sea floor, using a tripod to support the camera, the camera-to-object distance used in a survey ranges from 50 to 100 cm. The Ground Sample Distance (GSD) and the scene width (W) - i.e., the width of the area covered by the camera - were estimated using the following equations:

$$GSD = \frac{D}{f \cdot i}\, px_{size}\,; \quad W = \frac{D}{f \cdot i}\, w$$

where D is the distance between the camera and the object,
f is the focal length of the camera (8.7 mm for Rikola),
i is the refractive index of water (i= 1.34),
px_{size} is the pixel size of the sensor (5.5 µm),
w is the physical width of the sensor.

[1] Department of Environment, Land and Infrastructure Engineering of Politecnico di Torino.

[2] Department of Architecture and Design of Politecnico di Torino.

Using these parameters, the following values were obtained:

- At 50 cm:
    1. GSD ≈ 0.20 mm/pixel
    2. Image width (W) ≈ 24 cm
- At 100 cm:
    1. GSD ≈ 0.40 mm/pixel
    2. Image width (W) ≈ 50 cm

These values confirm that both image sharpness and spatial resolution are suitable for close-range imaging of underwater targets within this distance range. Depending on the specific application, the choice between 50 cm and 100 cm should be based on the trade-off between resolution and coverage area.

2.3 Data acquisition

The research is conducted along the northern coast of Sardinia, with two primary test sites: Culuccia Peninsula (October 2024) and Porto Conte Bay, Tramariglio (sampled in October and December 2024, respectively). Hyperspectral acquisitions were performed underwater, at depths of 5 and 15 m in Culuccia and 15 m in Porto Conte, and in air over collected PO samples in Porto Conte.

2.3.1 First campaign: Culuccia, October 2024: The first survey campaign of the underwater system was carried out on the 23rd to 25th of October 2024 in Culuccia, the testbed. During this survey, only underwater pictures were taken. The first test was performed at a depth of about 8 m, on a discontinuous PO meadow, while the second test was carried out at 15 m, the same depth as one of the steps of PO monitoring according to the ISPRA procedure.

The acquisition preparation involved creating a sequence of wavelengths to be recorded by a memory card inserted in the camera. The chosen sequence that was tested has the following characteristics:

1. Integration time: 40 ms for the first test, which resulted in images that were too dark, so 100 ms was chosen for the second and all subsequent tests.
2. Image size: 1010x1010 pixels, the maximum resolution the camera allows.
3. Sequence: from 506 to 904 nm with step 13nm (31 bands, 31.7 Mpix occupied on the memory card over 32), to record the whole spectrum of the camera and then analyse which bands are best. Table 1 shows the sequence of wavelengths used for the acquisitions presented in this research, which contains the band number, the central wavelength, and bandwidth (full width at half maximum - FWHM). This sequence allows to cover the entire spectral range of the camera.
4. Period: the interval of time between one photo and the next, which was 10 ms during the first test and was then increased to 15 ms. This period allows movement between two consecutive photos to acquire different objects and considers that the time required to capture a hypercube across all the spectral bands defined in the sequence above is about 4 seconds.
5. Delay: the shooting sequence begins after 10 minutes (600s) from the trigger to prevent taking photos during the descent phase of the dive.

Moreover, a tripod was used to have a steadier acquisition underwater; calibration panels from Mapir (Mapir, 2022) were used to post-process the images. The acquisition relies on at least two divers: one holds the camera mounted of a tripod and the other holds the third light and the calibration panels.

Sensor 1			Sensor 2		
Band	λ (nm)	FWHM (nm)	Band	λ (nm)	FWHM (nm)
12	649.02	6.42	1	506.31	7.68
13	661.82	7.03	2	519.11	7.45
14	675.08	7.41	3	532.09	6.68
15	687.92	6.55	4	545.15	5.93
16	701.34	6.73	5	558.28	7.2
17	714.43	4.92	6	571.31	5.69
18	727.01	4.16	7	584.07	5.73
19	739.95	4.93	8	597.24	6.56
20	753.12	4.44	9	610.07	7.57
21	765.79	3.65	10	622.97	7.04
22	778.95	6.37	11	634.83	6.73
23	792.03	6.25			
24	805.13	5.49			
25	817.58	9.55			
26	830.56	9.72			
27	844.23	8.99			
28	857.52	9.38			
29	869.54	9.21			
30	882.97	8.49			
31	896.21	9.12			

Table 1. Rikola sequences of wavelengths used for surveys.

2.3.2 Second campaign: Porto Conte Bay, December 2024: In December, another acquisition at a depth of 15 meters was conducted in the Bay of Porto Conte, refining the acquisition technique and testing new improvements to the UHI system (Figure 3). Specifically, a new black covering of the housing was applied to prevent light infiltration and reflection inside the case.

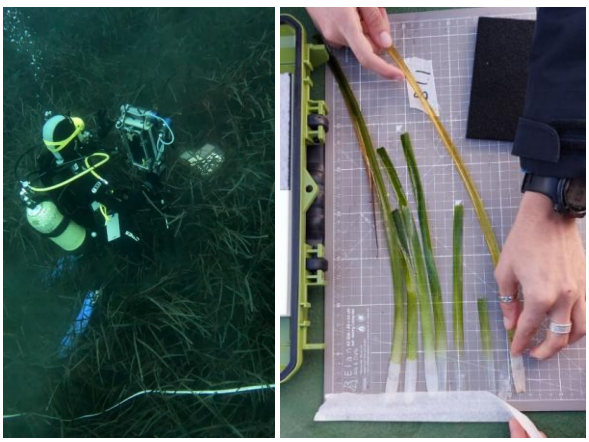

Figure 3. Underwater hyperspectral acquisition over a PO meadow (left). Hyperspectral acquisition out of the water on one of the PO bundles collected (right). Both pictures were taken on the 4th of December 2024 at Porto Conte.

The goal was to capture PO during an ISPRA-like monitoring procedure. The settings of the camera used an integration time of 100 ms, and the same 31 bands of the previous tests. The hyperspectral images were acquired on the PO on 3 quadrats 40x40cm along a transect of 20x5m. In the same positions, 3 PO bundles were collected in each of the 3 quadrats and acquired with the same hyperspectral camera out of the water, using the same 31 bands and integration time of 10 ms, being quite sunny. Also in this case, a tripod and Mapir calibration targets were used.

2.4 Hypercubes processing and PO spectrum estimation

After the hyperspectral image acquisition, the hypercubes are processed to perform radiometric calibration and to extract the spectral signature of Posidonia oceanica (PO), focusing on selected regions of interest (ROIs) within the images. This contribution describes only the processing of the *in-air* (or "dry") acquisitions. The primary objective of this preliminary analysis was to estimate the spectral signature of PO in the absence of water, thereby eliminating the complex effects of wavelength-dependent absorption and scattering caused by the aquatic medium.

The processing workflow begins with radiometric calibration, performed using the Senop Hyperspectral Imager software. Calibration employs both a dark reference (obtained by covering the lens with a black object at the beginning of each acquisition campaign) and a white reference target (a MAPIR Light Gray card with 65% reflectance). Following this, spectral extraction was carried out on ROIs, selected from different portions of the seagrass leaves, including green tissue, intermediate zones, and adult leaf sections. To derive a representative spectral signature, the spectra from all ROIs were averaged, and the standard deviation was calculated to assess variability across wavelengths. This provides insight into the spectral heterogeneity of PO at different physiological stages and can support future health status assessments.

3. Preliminary results

The underwater images acquired during the two field campaigns were, unfortunately, too blurred to be used in the current analysis. The first dataset, collected in October 2024, exhibited severe image degradation due to long exposure times and water movement. Although some improvements were implemented before the second campaign in Porto Conte, the images remained significantly affected by motion blur caused by the natural swaying of the seagrass in ocean currents and the long integration time required by the sensor. As a result, processing of the underwater data is still not feasible.

Future work will focus on refining the acquisition protocol to improve underwater image quality and include the detailed processing workflow for submerged acquisitions. The ultimate goal is to account for different PO health conditions, enabling spectral classification of tissue status under varying environmental conditions.

3.1 First campaign: Culuccia, October 2024 – Underwater imagery

The campaign in Culuccia, conducted in October 2024, served as the first test of the underwater hyperspectral imaging system. No "dry" photos of PO were taken out of the water in this campaign. This system was able to capture underwater hypercubes of PO at a depth of 15 meters. However, the images were very blurred and dark, making processing unfeasible. This effect is due to the natural movement inherent to the seagrass waving in the ocean currents, coupled with the long capture times of the camera and the intrinsic and physical characteristics of water, which absorbs light in a wavelength-dependent way, making infrared bands more absorbed than visible ones.

Nevertheless, the test was crucial in identifying issues related to the system and the acquisition technique, allowing for improvements in both. More in detail, the main considerations assessed after the test are as follows:

1. Blurry Photos. We observed that the time required for the camera to take a photo in each band is not short enough to prevent capturing the movement of the object, which, being PO leaves, moves with the waves.
2. Photos are darker as their wavelengths move towards the infrared bands. Looking at the hypercubes acquired, we noticed that the IR bands were often quite dark, meaning that the lights used were not powerful enough and not close enough to the object framed (Figure 4).
3. Vignetting and reflection marks. The hypercubes exhibited a vignetting effect, where the photo's edges appeared darker. This is likely due to the distance between the flat port and the lens. Reducing or avoiding this effect may be challenging because of the housing's construction constraints. Additionally, a circular bright mark was present in every hypercube, indicating a reflection from the lens (Figure 5).
4. The use of a square frame made from lightweight plastic provided a helpful approximation of the area being framed during image acquisition and the distance between the lens and the object (PO). In underwater environments, perception of distances is often distorted, especially for objects located less than 1 meter away.
   The camera operates in automatic mode, taking photos at set intervals indicated by an LED that flashes. However, due to the camera's housing, the LED is not visible. This makes the analysis of hypercubes very time-consuming, as it requires searching for the correct photo among many automatically taken images.

Figure 4. Example of a picture showing the insufficient light, especially in the background of the photo.

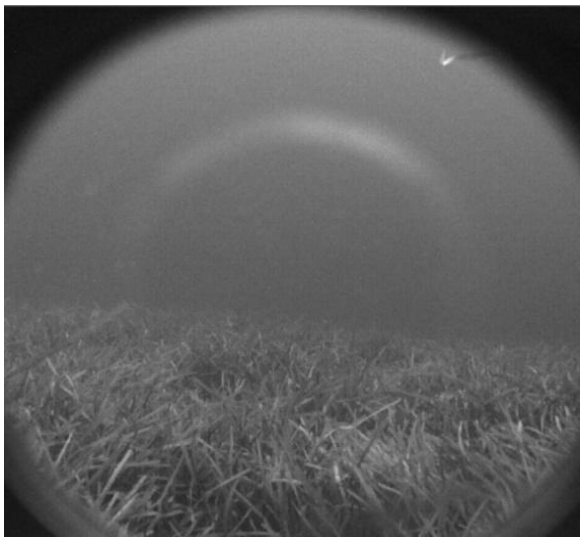

Figure 5. Example of a picture showing the vignetting effect.

3.2 Second campaign: Porto Conte Bay, December 2024 – Underwater and "dry" imagery

During the December 2024 campaign at Porto Conte Tramariglio, hyperspectral images of Posidonia oceanica (PO) were acquired for the first time in both underwater (at a depth of 15 meters) and aerial configurations.

Analysis of the underwater images indicated that some issues observed during the October 2024 test were successfully mitigated through the implementation of instrumental improvements described in the previous paragraph. Nonetheless, the underwater imagery remained significantly blurred due to the long exposure times combined with the natural movement of seagrass in ocean currents, thereby complicating further processing.

Here, the results of the "dry" image processing are discussed (Figure 6). The goal of this first analysis of PO hyperspectral images was to estimate its spectral signature as it is without the presence of a water medium, which interacts with light, absorbing specific wavelengths in various ways.

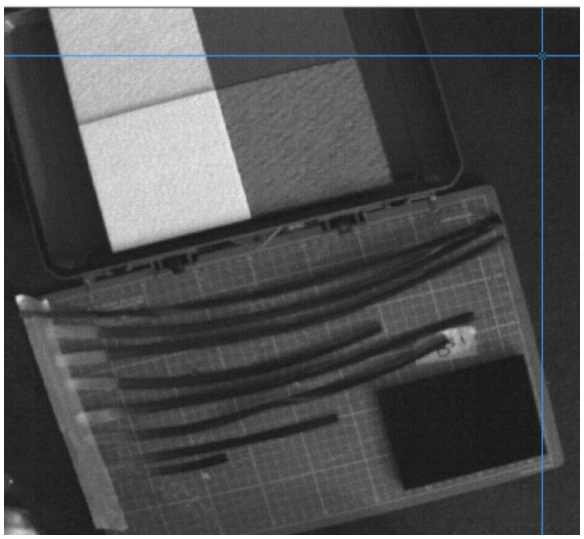

Figure 6. Example of hyperspectral image acquired out of the water on one of the PO bundles collected on the 4th of December 2024 at Porto Conte.

After the radiometric calibration on the Senop Hyperspectral Imager software, spectral extraction was performed on 35 regions of interest (ROI), each comprising a 3×3 pixel area (9 pixels per sample), for a total sampling area of 315 pixels. These ROI were taken from various parts of the leaves, including green tissue (green part of the leaf), intermediate, and adult leaves.

A representative spectral signature was then obtained by averaging the spectra of the ROIs, computing the standard deviation, the variability among for each wavelength can be understood (Figure 7).

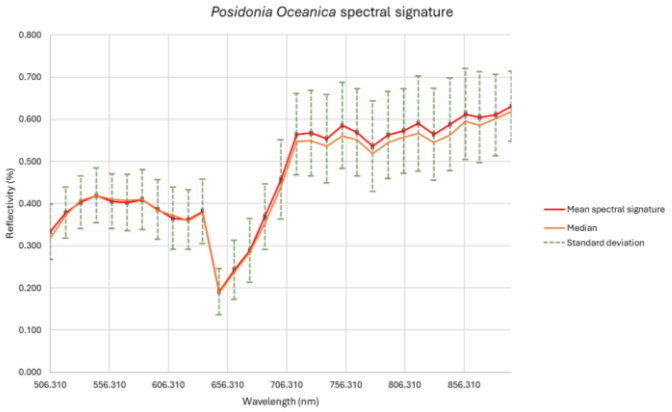

Figure 7. Estimated spectral signature of PO in "dry" conditions.

The spectral signature of Posidonia oceanica exhibits characteristics similar to those of terrestrial vegetation. In particular, a strong absorption in the red region of the spectrum is observed due to chlorophyll, resulting in low reflectance values, while a pronounced increase in reflectance is evident in the near-infrared (NIR) region, whose value is typically used as a proxy of vegetation health status. In the visible range, reflectivity typically hovers around 0.4, whereas in the NIR it increases to values between 0.55 and 0.65.

To identify the most significant wavelengths within the PO spectral signature, principal component analysis (PCA) was employed. PCA is a statistical method used to reduce the dimensionality of high-dimensional datasets while preserving the majority of their variability. It transforms the original variables into a set of orthogonal (uncorrelated) principal components or factors, with the first few components capturing most of the variance. In this study, PCA was performed using the XLSTAT add-in in Excel, employing a Spearman-based approach in which the data were standardized prior to analysis to prevent variables with high variances from unduly influencing the results. The PCA results are shown below.

The analysis revealed that the first three factors explain 95% of the variability in the dataset. Table 2 shows that band λ_{15} (687.9 nm) is strongly correlated with the first principal component (PC1), which accounts for 73% of the total variance among 31 bands, while band λ_{11} (634.8 nm) exhibited the strongest positive correlation with the second and third principal components (PC2 and PC3), explaining 21% and 2% of the variance, respectively. Considering instead the 99% of the total variance, the first 9 factors should be selected. Examining the scree plot (Figure 8), the "elbow" of the graph—the point at which the marginal contribution decreases significantly—is observed at the third principal component.

Bands	PC1 (73%)	PC2 (21%)	PC3 (2%)
λ_1 (506.3 nm)	0.702	0.607	0.124
λ_2 (519.1 nm)	0.824	0.540	-0.060
λ_3 (532.1 nm)	0.864	0.466	-0.080
λ_4 (545.2 nm)	0.880	0.433	-0.109
λ_5 (558.3 nm)	0.881	0.440	-0.079
λ_6 (571.3 nm)	0.852	0.510	-0.028
λ_7 (584.1 nm)	0.834	0.539	0.006
λ_8 (597.2 nm)	0.844	0.519	0.041
λ_9 (610.1 nm)	0.857	0.495	-0.001
λ_{10} (623 nm)	0.829	0.535	0.083
λ_{11} (634.8 nm)	0.521	**0.707**	**0.388**
λ_{12} (649 nm)	0.838	0.423	-0.228
λ_{13} (661.8 nm)	0.852	0.403	0.090
λ_{14} (675.1 nm)	0.868	0.395	-0.069
λ_{15} (687.9 nm)	**0.939**	0.079	-0.257
λ_{16} (701.3 nm)	0.904	-0.301	-0.237
λ_{17} (714.4 nm)	0.911	-0.372	-0.026
λ_{18} (727 nm)	0.852	-0.488	-0.033
λ_{19} (740 nm)	0.830	-0.520	-0.040
λ_{20} (753.1 nm)	0.846	-0.429	0.016
λ_{21} (765.8 nm)	0.875	-0.459	0.049
λ_{22} (779 nm)	0.846	-0.487	-0.094
λ_{23} (792 nm)	0.870	-0.460	-0.022
λ_{24} (805.1 nm)	0.894	-0.415	0.057
λ_{25} (817.6 nm)	0.790	-0.409	0.302
λ_{26} (830.6 nm)	0.897	-0.404	0.076
λ_{27} (844.2 nm)	0.879	-0.430	0.081
λ_{28} (857.5 nm)	0.885	-0.395	0.022
λ_{29} (869.5 nm)	0.892	-0.405	0.029
λ_{30} (883 nm)	0.919	-0.338	0.055
λ_{31} (896.2 nm)	0.923	-0.241	0.154

Table 2. Correlation between wavelengths and principal components.

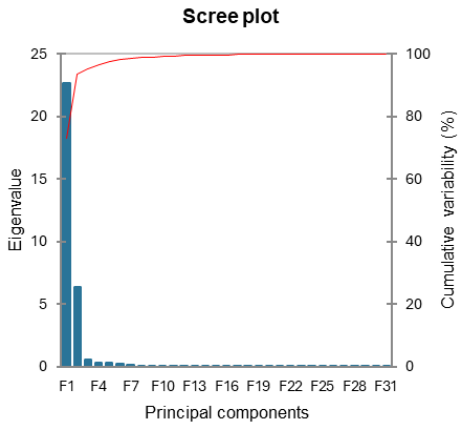

Figure 8. Scree plot of the principal component analysis.

As a result, in this preliminary study, the first three factors are currently considered: λ_{15} and λ_{11} could be candidate bands to focus on for further analysis regarding PO. In the next steps of this project, this analysis could assist in selecting the most significant wavelength bands to define a spectral index for analyzing the PO health status.

Based on the results obtained from this preliminary analysis of the hyperspectral data, future efforts will focus on defining health status indicators for PO. Further investigations will be required to explore spatial patterns of plant community structure, identify functional vegetation types, and potentially discriminate other submerged macrophytes coexisting with PO.

4. Improvements and future work

4.1 UHI System Design

As mentioned in the Preliminary results section, the two main challenges this study faced include image blurring due to the movement of seagrass and light absorption by water, with darkness especially in infrared bands. Knowing that, the improvement process started with the following steps:

1. To define the time needed to capture the entire sequence of wavelength, we timed the acquisition in lab, using the same sequence of wavelength used in field: an integration time of 100 ms, with 31 wavelengths ranging from 506 to 904 nm in 13 nm steps and a time step of 15 seconds between two hypercubes. The test showed that the time to capture one hypercube is 4 seconds. This time gives an indication of the stability required for the acquisition setup. To cope with the stability issue, we experimented with different configurations of the tripod, aligning its central axis horizontally and vertically. However, capturing static photos remained challenging. Even slight movements from the plant's leaves amplify this problem. The absence of a monitor to display the framing area and the lack of a physical button to take photos, as we are using an automatic acquisition mode, necessitate maintaining a steadier camera position. Ultimately, we decided to replace the tripod with a structure inspired by the one used in the project “Under the pole” (UNDER THE POLE, 2010) The structure's design is the one shown in Figure 9 and construction is still in progress, expected to be ready for the first campaign in June 2025. It will be tailored to ensure stability, manoeuvrability, and optimal control of distance and angle relative to the seabed during hyperspectral image acquisition.
2. To tackle the darkness observed in IR bands, we tested new lights, more powerful in terms of lumens. They are from Easy Dive company and composed of LEDs that light up infrared bands (Easy Dive, 2024). Preliminary testing is undergoing in the department’s pool (Figure 10), and the full light system will hopefully be implemented in the 2025 field survey. The goal is to improve illumination uniformity and spectral coverage, especially in deeper or turbid environments.
3. To understand how to eliminate the circular reflections in our photos, experiments in the lab were conducted. We took pictures using both a covered housing, which prevented light from entering, and an uncovered housing, as was utilized during the October test in Culuccia. The comparison revealed that the covered setup exhibited no visible reflections, whereas the uncovered housing still showed circular reflections. This finding allowed us to enhance the

housing by applying an opaque black coating, which prevents light infiltration and propagation through the otherwise transparent plexiglass.

4. In order to smooth and speed up the visualization of the photos after the survey, we added to the housing a stopwatch that displays the current time or elapsed time from the start of the acquisition. This would help locate specific photos by noting the time on an underwater writing dive slate.

Figure 9. Design of the new structure that supports the Rikola camera, its housing and lamp: the Underwater Hyperspectral system.

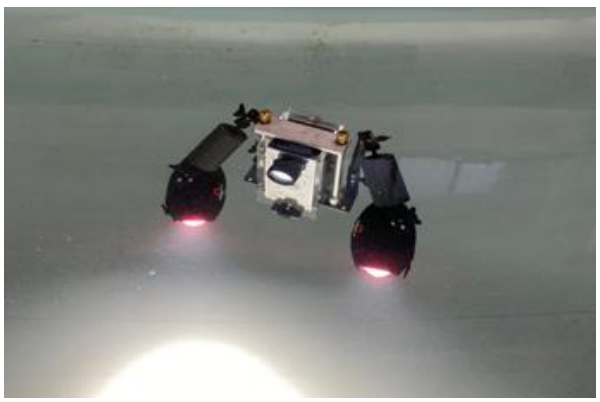

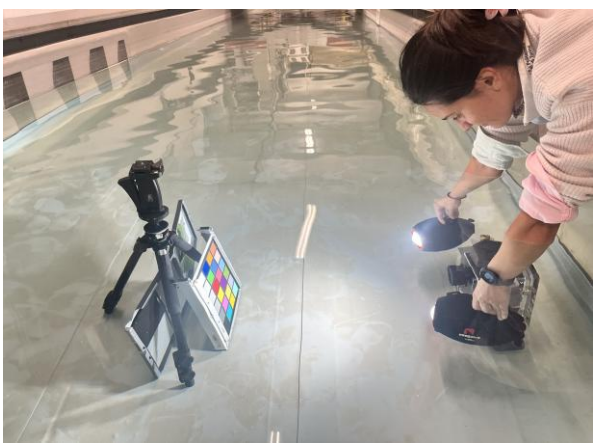

Figure 10. Testing of the new lights in the shallow testing pool of Politecnico di Torino.

4.2 Hyperspectral Image Processing

The next phase of the project will include further development of the hyperspectral image processing pipeline, extending the workflow currently applied to “dry” acquisitions to underwater imagery. Additionally, vegetation index development will be explored to extract ecological indicators from the hyperspectral data. Based on the results obtained from this preliminary hyperspectral data analysis, future work will aim to develop quantitative indicators of the health status of *Posidonia oceanica*, derived from its spectral properties. In particular, the identification of key wavelengths — as highlighted through Principal Component Analysis — may serve as the foundation for designing a dedicated spectral index capable of detecting physiological stress, degradation, or recovery trends in PO meadows. Such indices could be validated against traditional indicators of plant health, such as pigment concentration, phenol content, or chlorophyll fluorescence parameters.

5. Conclusions

Despite the technical difficulties encountered, these preliminary tests provided critical insights into system limitations and acquisition methodology, paving the way for future improvements. This contribution will describe the preliminary methodology developed, involving the instruments and the acquisition technique; the first results and lessons learned from the hyperspectral imaging tests; the strategies for optimizing acquisition techniques to enhance underwater hyperspectral data quality.

By sharing these findings, the authors aim to foster fruitful discussions with the research community, exchange expertise, and refine methodologies for future applications in underwater hyperspectral mapping.

Acknowledgements

Poseidon is a research project of Italian national relevance initiative “Italia Domani - Piano Nazionale di Ripresa e Resilienza” (PNRR) funded by the European Commission - Next Generation EU.

The partners extend their gratitude to BIRU srl (Culuccia) and the Marine Protected Area of Capo Caccia – Isola Piana for their hospitality within their respective areas of jurisdiction and for their valuable collaboration in supporting the project.

References

Costa, V., Serôdio, J., Lillebø, A.I., Sousa, A.I., 2021. Use of hyperspectral reflectance to non-destructively estimate seagrass *Zostera noltei* biomass. Ecol. Indic. 121, 107018. https://doi.org/10.1016/j.ecolind.2020.107018

Dumke, I., Nornes, S.M., Purser, A., Marcon, Y., Ludvigsen, M., Ellefmo, S.L., Johnsen, G., Søreide, F., 2018. First hyperspectral imaging survey of the deep seafloor: High-resolution mapping of manganese nodules. Remote Sens. Environ. 209, 19–30. https://doi.org/10.1016/j.rse.2018.02.024

Easy Dive, Revolution Hyperspectral light, 2024 https://www.easydive.it/blog/invenzioni/2024-revolution-hyperspectral.124.html (20 May 2025)

Foglini, F., Grande, V., Marchese, F., Bracchi, V.A., Prampolini, M., Angeletti, L., Castellan, G., Chimienti, G.,

Hansen, I.M., Gudmundsen, M., Meroni, A.N., Mercorella, A., Vertino, A., Badalamenti, F., Corselli, C., Erdal, I., Martorelli, E., Savini, A., Taviani, M., 2019. Application of Hyperspectral Imaging to Underwater Habitat Mapping, Southern Adriatic Sea. Sensors 19, 2261. https://doi.org/10.3390/s19102261

Johnsen, G., Ludvigsen, M., Sørensen, A., Sandvik Aas, L.M., 2016. The use of underwater hyperspectral imaging deployed on remotely operated vehicles - methods and applications. IFAC-Pap., 10th IFAC Conference on Control Applications in Marine SystemsCAMS 2016 49, 476–481. https://doi.org/10.1016/j.ifacol.2016.10.451

Kišević, M., Smailbegović, A., Gray, K.T., Andričević, R., Craft, J.D., Petrov, V., Brajčić, D., Dragičević, I., 2011. Spectral reflectance profile of Caulerpa racemosa var. cylindracea and Caulerpa taxifolia in the Adriatic Sea. Acta Adriat. 52, 21–28.

Mapir, M., n.d. Diffuse Reflectance Standard Calibration Target Package (V2) [WWW Document]. MAPIR CAMERA, 2022. URL https://www.mapir.camera/en-gb/products/diffuse-reflectance-standard-calibration-target-package-v2 (30 September 2024).

Mazzuca, S., Spadafora, A., Filadoro, D., Vannini, C., Marsoni, M., Cozza, R., Bracale, M., Pangaro, T., Innocenti, A.M., 2009. Seagrass light acclimation: 2-DE protein analysis in *Posidonia* leaves grown in chronic low light conditions. J. Exp. Mar. Biol. Ecol. 374, 113–122. https://doi.org/10.1016/j.jembe.2009.04.010

Mills, M.S., Ungermann, M., Rigot, G., den Haan, J., Leon, J.X., Schils, T., 2023. Assessment of the utility of underwater hyperspectral imaging for surveying and monitoring coral reef ecosystems. Sci. Rep. 13, 21103. https://doi.org/10.1038/s41598-023-48263-6

Tommaselli, A.M.G., Berveglieri, A., Oliveira, R.A., Nagai, L.Y., Honkavaara, E., 2016. ORIENTATION AND CALIBRATION REQUIREMENTS FOR HYPERPECTRAL IMAGING USING UAVs: A CASE STUDY. Int. Arch. Photogramm. Remote Sens. Spat. Inf. Sci. XL-3-W4, 109–115. https://doi.org/10.5194/isprs-archives-XL-3-W4-109-2016

UNDER THE POLE project, 2010, https://underthepole.org/ (20 May 2025)

Vassallo, P., Paoli, C., Rovere, A., Montefalcone, M., Morri, C., Bianchi, C.N., 2013. The value of the seagrass Posidonia oceanica: a natural capital assessment. Mar. Pollut. Bull. 75, 157–167. https://doi.org/10.1016/j.marpolbul.2013.07.044